SCHOOL OF PHYSICS

FINAL YEAR PROJECT, DISSERTATION OR PHYSICS EDUCATION REPORT

NAME:	**William Foxall**
COURSE:	**BSc Physics**
PREFIX	**F300**
TITLE:	**Calibration of the Coldrick Observatory's Optical Telescope**
YEAR OF SUBMISSION:	**2011**
SUPERVISORS:	**Ben Maughan & Rhys Morris**
NUMBER OF WORDS:	**9009**

School of Physics
Tyndall Avenue
Bristol BS8 1TL

2010/11

DECLARATION

Due to the nature of the project, substantial preparation work leading up to a number of joint nights of observations on the telescope, the majority of the work prior to observing was done in a very collaborative manor and very little was performed individually.

All physical data (CCD testing and night observations) were taken together although sometimes in alternate shifts as some were lengthy (such as the 20 half hour exposures of dark current).

After the observing data was obtained Richard Painter and I each performed our own data analysis. We did, however, split the process of researching the photometry method between us. Richard compiled the conversion formulae to work from B and V magnitude values of stars to a theoretical r' magnitude. I worked on obtaining an experimental value for magnitude with the Aper function and wrote the code for an IDL function based on the principle (but not the actual code) of the Aper function in order to obtain errors for the flux values.

Richard and I both wrote our own mask based pixel fixing IDL routines. Mine, 'Maskfix' is displayed in the Appendix of this report.

The method of obtaining an extinction coefficient by producing the plot in Figure 13 was also a development of mine during my data analysis.

I also found, researched and attempted the method of looking for bias frame noise with a FFT along with devising the methods of bad pixel masking we called 'warm' and 'cool' masking.

Richard noticed the light leakage of the CCD, its trend with failing ambient light and promptly suggested we move to the darkroom significantly increasing the reliability of our dark current analysis.

CONTENTS

Acknowledgements

During the course of this final year project, near weekly meetings with Ben Maughan and Rhys Morris have proved invaluable and I would like to thank them both for all the time and effort they've put into helping Richard and myself and for the interest they've paid to the work we've been doing.

I'd also like to thank Paul Giles and Alex Lockey for staying late in the physics department as supervisors on our nights of observations.

ABSTRACT

The Bristol Physics Department's Coldrick Optical Observatory was explored and its potential to take scientific data analysed. The process was performed through extensive testing of the CCD camera and its pixel defects in lab conditions, along with two nights' observing. A full photometry calibration was performed and IDL functions compiled to enable this goal to be achieved. The observatory's potential for measurements in seeing, angular separation and photometry were quantified.

1. INTRODUCTION

The Coldrick Observatory at the H.H. Wills Physics Laboratory was gifted to the department by Bristol graduate William P. Coldrick [1]. Included in the observatory is an optical telescope dome featuring an alt-azimuth mounted Meade 10” LX200 reflecting telescope and a Santa Barbara Instrument Group ST-7E CCD camera.

The optical observatory has not been in frequent use for some years with the exception of a similar project performed last year in which the raw potential of the dome was explored. This project has aimed to expand upon the groundwork set by the 2009-10 students and has looked deeper into the capability of the CCD as well as the restrictions present due to the observatory’s location in Bristol and telescope setup.

As a secondary aim some basic observations were conducted through a Sloan r’ filter in order to trial the completed calibrations and to ascertain if the practical limitations of the setup agree with those of the theoretical predictions.

2. DETAILED BACKGROUND

THE TELESCOPE:

SCHMIDT-CASSEGRAIN DESIGN.

The Meade LX200 is a 10” Schmidt-Cassegrain reflector, a design based on a classical Cassegrain and popular for amateur astronomy [2]. A schematic of its design is shown below in **Figure 1**. It differs from the classical design by several added features. Most importantly it incorporates a spherical primary mirror instead of the parabolic employed in the classical design. Since a spherical mirror does not focus to a point, the LX200 features a thin lens (2-sided aspheric correcting plate) that enables it to focus correctly [3].

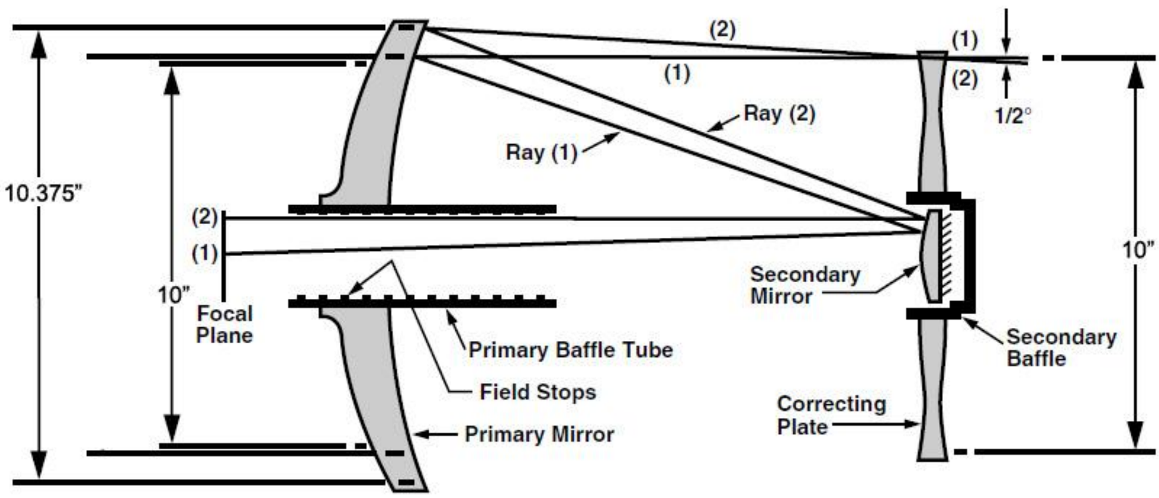

Figure 1 – A design schematic of the LX200 8” telescope. The aperture dimensions have been edited to match those of the LX200 10” model. *(Image credit: Meade Instruments)* **[3]**

The benefit of the oversized primary mirror is a wider fully illuminated field of view. Off axis illumination is increased by 10% compared to a standard 10” primary mirror [3]. To illustrate this point, one will notice that ray 2 in **Figure 1** would be lost with a 10” primary. Generally, one would keep the observed object as centred at the focal plane as possible but this oversized mirror increases the reliability of photon counting at an arbitrary point in the field of view.

MOUNT & COORDINATE SYSTEMS

The locations of stars in the sky are described in one of the coordinate systems employed by astronomers. Each of these is quantified by two angles about perpendicular axes at the centre of the ‘celestial sphere’, a very large hypothetical sphere centred on the Earth upon which it can be considered the stars sit.

The LX200 in the observatory sits mounted in the altitude-azimuth configuration where one axis of rotation, azimuth, rotates about circles that lie on the celestial sphere parallel to the observers horizon. The other axis of rotation, the altitude, draws circles perpendicular to the horizon that pass through the zenith (the point directly above the observer).

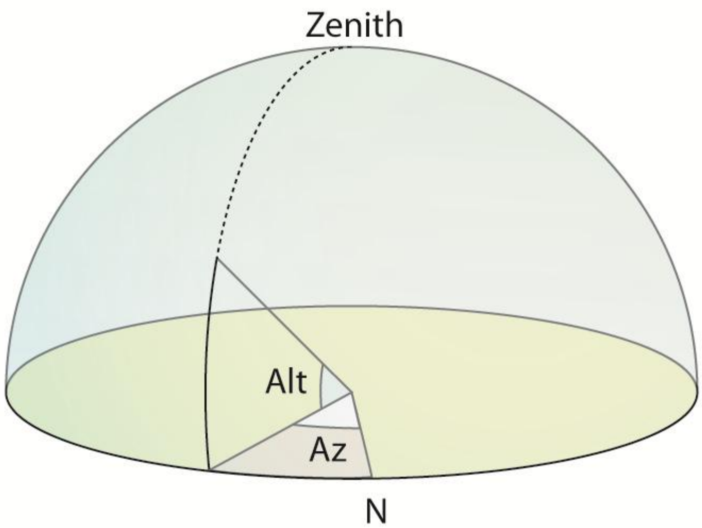

Figure 2 – The Horizon/Alt-Az system on the celestial sphere. Azimuth (Az) is measured East from North while altitude is measured from the horizon to the zenith on a great circle such that the zenith is 90°.

Due to the rotation of the Earth, the stars appear to move around circles on the celestial sphere. As a result, in the horizon system the altitude and azimuth of a star will change with time. An alternative treatment is to consider the Earth as static and the celestial sphere to rotate about the Earth’s projected axis. Another coordinate system that makes use of this analogy is the equatorial system in which a unique point on the celestial sphere is describes by the angles of right-ascension (RA) and declination (Dec). The celestial poles and equator are just the projection of the Earth’s axis and equator onto the celestial sphere respectively.

The right-ascension is measured in the plane of the celestial equator from the first point of Aries (♈), the point at which the sun crosses the celestial equator at the vernal equinox (approx. 21st March). Declination is measured from the celestial equator to the north such that the north celestial pole is at 90° and the south celestial pole is -90° [2].

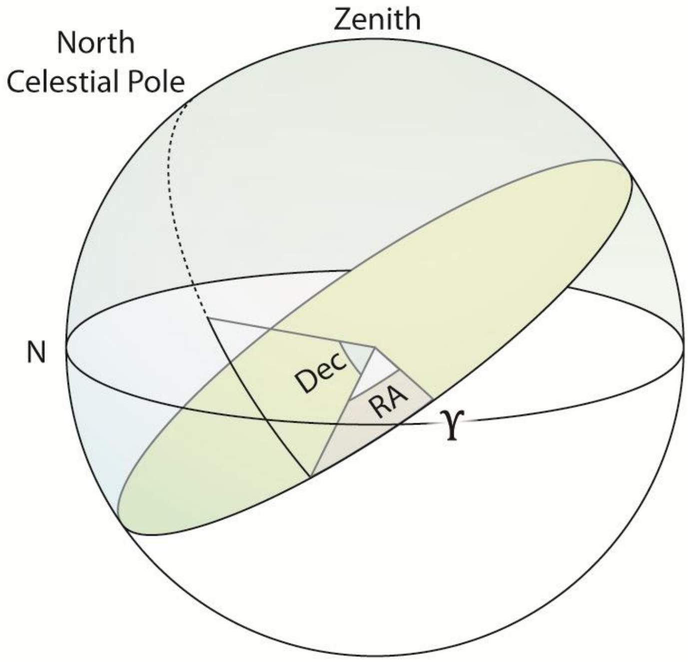

Figure 3 – The equatorial system superimposed on the horizontal system. The observer's horizon is horizontal while the celestial equator is at an angle to this.

The equatorial system is useful and is used extensively by astronomers because the right-ascension and declination of a star is constant since the entire coordinate system rotates with them. The LX200 moves on its alt-az mount but tracks the equatorial system.

A WORD ON ABERRATIONS

Telescopes always suffer from aberrations of various types that cause the image through them to deviate from a true representation of the subject being viewed. A reflecting telescope such as the LX200 is immune to chromatic aberration, an effect that arises from the wavelength dependence of the light's path through a lens, where light of varying wavelength focuses along a line rather than at a point.

Important aberrations that do occur in a reflecting telescope are spherical and coma. Spherical aberration occurs when a spherical mirror is used. Light reflected closer to the centre of the mirror will be focussed further away than light arriving at the edges of the mirror. The Schmidt-Cassegrain design of the LX200 uses a spherical mirror and so the thin correcting lens is used to counter the spherical aberration. Coma is an off axis aberration that is the result of varying magnification depending on the angle of incidence on the mirror. It's an intrinsic property of a parabolic mirror. The Schmidt-Cassegrain again reduces this effect by making use of spherical primary mirror, correcting lens and hyperbolic secondary mirror [4].

SDSS r' BAND FILTER

The Coldrick Observatory owns a SDSS (Sloan Digital Sky Survey) r' filter which transmits a specific portion of the visual light range centred on $\lambda = 623.1\ nm$ (red light) [5]. The application this presents is a way of standardizing photometry performed in the observatory. Photon counts can be recorded for a particular star through the filter and then compared to a literature value through the same filter band at another observatory.

Diffraction Limit

When the light from a point-like source passes through a circular aperture the characteristic diffraction pattern of concentric rings is observed. The bright central core is known as the Airy disk (named after the English physicist George Airy).

Lord Rayleigh, an English physicist of the late 19th century, reasoned if two diffraction ring patterns from close in proximity point-like sources are observed, the low limit at which they can be discerned as separate sources occurs when the centre of one airy disk falls into the first minimum of the other's diffraction pattern. This is described by the following expression [2]:

$$\sin\theta = 1.22\left(\frac{\lambda}{d}\right)$$

For the LX200's 10" aperture, this expression gives a diffraction limit in the r' band of 0.62 arc seconds.

The CCD

The CCD, or charge-coupled device, has transformed the potential of astronomy. Prior to its use chemical photography was the only method, short of sketching your view, of recording observations. The first image was a daguerreotype taken in 1840 by J. W. Draper; the subject was the Moon. 135 years later the first astronomy image with a CCD camera was taken [2].

How a charge-coupled device works

The advantage of the operation of a CCD is its ability to record accumulated light intensity in numerical form as a function of position rather than with film where the intensity of light is just represented through chemical processing.

The construction of a CCD consists of a p-n semiconductor junction, electrode conductors (three per imaging pixel) and a thin insulating layer separating the electrodes from the junction. Due to the concentration differences of electrons and holes in the n and p regions respectively (a hole can be considered as a lack of a photon or a corresponding positive free charge carrier) a space-charge zone is formed with exposed positive ion cores on the n side and negative ions on the p side. This favours the movement of any electrons in the conduction band of the p side to the n side to minimise its potential energy [6].

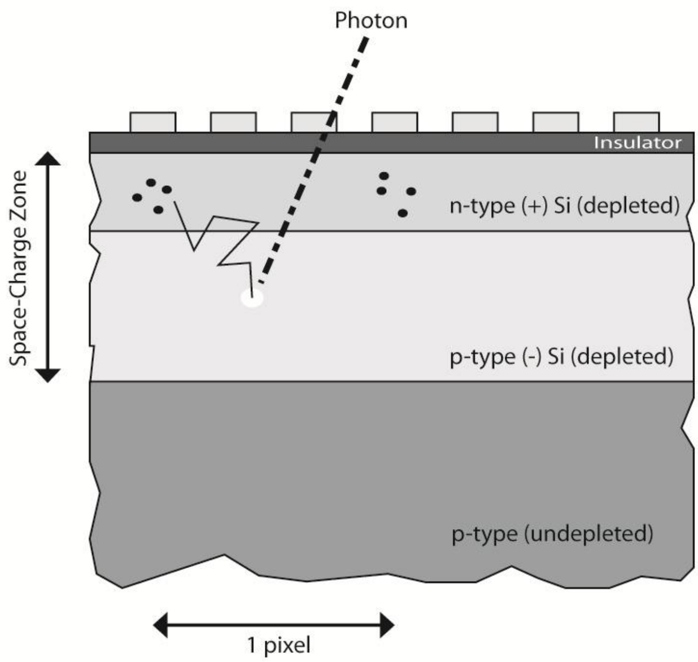

Figure 4 – A schematic of the structure of a small portion of a CCD. A photon enters the depleted p-type region of the space-charge zone before exciting a photoelectron into the conduction band causing it to meander to the n-type side under the current charged electrode, where the photoelectron's potential energy is lowest.

Prior to an exposure of the sky the n-type region is cleared of any electrons with an electric field. Then, as illustrated in **Figure 4**, when a negative ion in the p region is exposed to a photon it donates an electron to the conduction band. This photoelectron then favours moving up into the n region due to the potential gradient. When a potential is applied to an electrode, the photoelectrons accumulate underneath it where their potential energy is lowest.

Following exposure the charge accumulated at each pixel needs to be counted. This is performed in a shuffling manor. The voltage applied to the electrodes are varied along the rows in groups of three such that in each cycle the charge on one pixel is moved along one and the charge in the end pixel is dumped into a column called the transfer register [6].

After each shuffle cycle the charge of each pixel in the transfer register is read out with a field-effect transistor into an analogue-to-digital converter. The digital data is then stored in a computer one column at a time and later combined to form a whole image.

The amplitude of the signal from the field-effect transistor is proportional to the charge in the corresponding pixel being read out. In turn this is proportional to the number of photons detected by that pixel. The digital output of this value is a quantised number known as counts. The constant of proportionality relating this value to the number of electrons is known as the gain and is an important value that is dependent on the CCD design as, due to one electron corresponding to one photon, it tells us how many photons a particular count value corresponds to.

If the exposure is long enough, the number of photoelectrons collecting under the charged electrode may exceed the amount the potential well can contain and as a result further electron accumulation would be able to 'spill' over to a neighbouring pixel along the row. This is known as blooming. Also, at high photoelectron accumulation, the pixel may begin to lose charge to recombination of electrons and holes; charge collection becomes nonlinear with time. The point at which this 'saturation' occurs is called the full-well capacity [2] [7].

SOURCES OF NOISE

Not all the charge accumulated at a pixel will be from the source that is being observed and often the pixel will count fewer photons than we would expect too. Unwanted photon counts (or lack of) come from a variety of origins; dark current, CCD bias, flat field, read noise and shot/Poisson noise.

Dark current is an additive form or noise that accumulates with time and arises due to the thermal photons emitted by the surroundings, predominantly by the CCD housing. This is reduced with decreasing temperature and as a result most CCD cameras used for astronomy include cooling systems.

CCD bias is a characteristic quality of each individual device. It should be the same with each exposure regardless of length and as such is characterised by a zero-second exposure. It is caused by the zero point of charge for each individual pixel and may contain structure across the image.

The optics of any telescope system are never perfect and uniform illumination across the entire field of view is generally unobtainable. The flat-field noise quantifies this. Some areas of the field may consistently experience a reduced photon count while others may experience more, this can be due to diffraction or reflection in the optical system, dust or external light leaking in [8].

The CCD's analogue-to-digital converter has a resolution associated with it. This can be considered as a source of noise. The higher the resolution of the converter, the lower the chance of a photon count being missed of fabricated. This is called digitalization noise and is calculated as [2];

$$\sigma_{dig} = \sqrt{\frac{g^2 - 1}{12}}$$

Digitalization noise is one contributor to the electronic random noise known as read noise. This category includes Johnson noise, reset noise and flicker [9]. The CCD manufacturer usually quotes the R.M.S. value of read noise in their product documentation.

Shot/Poisson noise is unavoidable source of noise that is the result of the statistical nature of photon counting. It follows well understood Poisson statistics such that the expected error in any reading of N photon counts is simply $\sqrt{N}$.

NYQUIST LIMIT

As well as the telescope aperture's diffraction limit, the discrete pixels in a CCD provide another limitation on the angular resolution. The minimum level of detail that can be resolved from a CCD image is differing values of two adjacent pixels. Therefore the minimum angular resolved angle is equal to the corresponding angle that 2 pixel widths subtend on the sky.

THE SBIG ST-7E

The Coldrick Observatory's ST-7E is a 765 by 510 pixel front-illuminated CCD camera with cooling capable of 30°C below ambient temperature. The analogue-to-digital converter is 16 bit and so has a possible 65536 levels. Its gain is 2.3 electrons per analogue-to-digital unit (or ADU) which gives a digitalization noise of 0.60. The overall read noise is quoted in the documentation as 15 $e^{-}\ rms$. The quantum efficiency of the Kodak sensor is quoted at 60% for the red filter band. This means that 60% of photons with that particular frequency that fall incident on the detector will be included as counts [10].

CCDOps

SBIG's camera interfaces with the computer through a parallel port and with the software CCDOps. Exposure time, operating temperature, dark frame settings and other settings are controlled from the software interface. After an exposure has been taken the image, histogram of intensities and individual pixel values can be viewed.

CCDOps also facilitates in the telescope focussing procedure when the CCD is attached. A low resolution exposure can be repeatedly downloaded from the camera to view, in near real-time, the adjustments being made to the focussing. The peak value is also displayed which gives an indication of focussing since when the full-width half maximum of a star's point spread function (the Gaussian-like intensity distribution a point source appears as on the sky through optics) is at its smallest (optimum focussing) the peak value is also at its greatest.

The Effects of the Atmosphere on Observations

Ground based observations have to contend with the multiple ways in which the atmosphere affects the light reaching our observatories. The optical band, in which we see, is a rare window of transparency of the frequency spectrum for atmosphere. This is why we have evolved to be sensitive to these wavelengths. Astronomers view the sky in a much wider spectrum, fortunately the observations in the r' filter in this project fall within this window of transparency. However, the following effects are also to be considered.

Extinction

A very important consideration when performing photometry, extinction can significantly decrease the apparent magnitude (or instrumental magnitude) of the observed light source. Water drops or dust particles in the air absorb some of the light between the source and the telescope. The effect is least apparent when looking directly upwards as you are looking through less of the atmosphere. Towards the horizon it is at its worst as there is a large air mass in your line of sight.

The effect is therefore dependent on the altitude of the object in the horizon system. An approximate expression for the air mass can be used at angles of less than 60° from the zenith;

$$X = \sec z$$

where $\boldsymbol{X}$ is the air mass and $\boldsymbol{z}$ is the angle measured from the zenith.

The expression is an approximation since it doesn't take into account refraction of the light entering the atmosphere nor the curvature of Earth. The full expression is [2]:

$$X = \sec z \left(1 - 0.0012(\sec^2 z - 1)\right) \quad \textbf{(1)}$$

The magnitude of a star is then corrected by subtracting the air mass multiplied by a coefficient of extinction for the observed frequency band from the instrumental magnitude recorded:

$$m_{\lambda 0} = m_\lambda - k_\lambda X \quad \textbf{(2)}$$

where $\boldsymbol{m_{\lambda 0}}$ is the corrected apparent magnitude, $\boldsymbol{m_\lambda}$ is the observed instrumental magnitude and $\boldsymbol{k_\lambda}$ is the coefficient of extinction for the observing frequency band.

Seeing

Treating the atmosphere as a composition of 'cells' of air, each with differing refractive indices, it becomes clear that their random movement would provide an unpredictable image blurring and motion. A star may appear to move around randomly on the sky, change shape or even break up and recombine again. These fluctuations are quite fast and are only obvious when viewing manually with the eyepiece or with a very short exposure.

A regular length to longer exposure will display the average of these fluctuations. The resulting image is known as the seeing disk. It is a two-dimensional Gaussian, the full-width half maximum (FWHM) of which gives us a measurement of the seeing. The smaller the FWHM, the better the seeing and the higher the potential of the setup to resolve smaller features (diffraction limit permitting). Seeing is considered to be excellent when the seeing disk is approximately 1 arcsec and poor when it reaches a value as high as 10 arcsecs [2].

As the seeing does not change the number of photons collected from the source it doesn't hinder any ability to perform photon counting photometry observations.

Scintillation

Scintillation is closely related to seeing as its cause is also the fluctuations of air pressure in cells. As the refracted light changes path constantly, the observer experiences moments of lower and higher intensity. With longer exposures this effect averages out and does not degrade the quality of the image, however care must be taken if one were to perform photometry on a short exposure. The solution would be to add several single exposures in order to hope to manually average out the effect through post processing [2].

Scintillation also varies with the angular size of the object. Larger objects subtend an air pocket larger than the fluctuations in the air and as such average out over the space they occupy. The effect is more pronounced with the distant stars that subtend a very small angular size.

Cloud Cover

Of course the cloud cover also dictates the amount of light that one detects from a source, it also scatters the light away from a direct path and so also has the effect of increasing the FWHM. A night may appear to have excellent seeing at first glance but when measurements are taken even a very thin uniform layer of cloud may present a significantly increased FWHM.

Conditions under which photometry cannot be accurately performed are said not to be photometric. There is no formal classification for what defines photometric conditions or not. However if one were to define a degree of acceptable loss of flux from a star of known output, they could go about marking their own classification.

ASTRONOMY METHODS

MAGNITUDES

The brightness of an object is often measured in a logarithmic scale called magnitudes. The scale is reverse such that negative magnitudes are brighter sources than positive magnitudes. Going up one magnitude is equivalent to decreasing the flux of photons from the source by the 5th root of 100. This is because when the scale was designed it was decided that a difference of 5 magnitudes should imply a factor of 100 in the flux. A constant, C, is then decided on such that an object of particular flux corresponds to magnitude $m = 0$. This provides the Pogson equation [2]:

$$m = -2.5 \log F + C \tag{3}$$

where F is the flux received and m is the magnitude.

SIGNAL-TO-NOISE RATIO

The signal-to-noise ratio or SNR is simply the ratio of the number of counts associated with the object being observed (signal) to the data's noise. A lower SNR image makes it harder to obtain a reliable value for any photometry where the goal is to find the signal counts. The error in the value decreases with increased SNR [2].

IMAGE SCALE

The dimensions of a CCD image when imported to the computer through CCDOps are only stored in pixels. Therefore it's important to know what real sky angle a pixel width corresponds to when analysing any angular separations in your image. The image scale is the size of one pixel as an angle on the sky and is defined by:

$$S_I = \frac{206.265\mu}{f} \tag{4}$$

where μ is the pixel size in microns and f is the focal length of the telescope in mm.

3. Experimental

The aim of the experimental work was to obtain data sufficient to provide as comprehensive a model of the CCD's behaviour as possible with varying temperature, exposure length, incident flux and any other variables that might occur during a night's observing.

Data Manipulation

Image data downloaded from the CCD camera is analysed on the computer in a Linux run programming environment commonly used by astronomers called IDL or Interactive Data Language. This programming package easily handles FITS (Flexible Image Transport System) files, the format in which the files are downloaded from the CCD.

FITS files are particularly useful for CCD image analysis as they consist of the rawest form of the charge collection data along with a header that includes all the additional information about the particular observation such as the date and time it was taken, the CCD temperature and the name of the astronomer that took the observation. The main body of the data takes the form of a simple 2D array with dimensions that match the pixels on the CCD. So for the ST-7E the files are arrays of 765 by 510 with the number of ADUs counted for each pixel. This array can then be read into a standard programming language floating point, integer array or similar. In the case of this experiment the language used was that of IDL.

Darks, Flats and Bias

For a standard frame of the sky the standard procedure is to apply 3 correction images known as dark, flat and bias frames. Their aim is to each address the specific sources of noise after which they are named and that were discussed in the previous section of this report.

Bias Frames

For the experimental work in this project, several bias frames were taken on the shortest exposure length possible (0.12 seconds), the frames were then median filtered. This is simply taking the median value for each pixel across all the files and placing it into the corresponding pixel of a new 765 by 510 array.

One must also be sure that the 0.12 seconds of exposure do not contribute any pixel counts on top of the CCD bias for each frame. To ensure this was the case two steps were taken. Firstly, all bias frames were taken without any light exposing the CCD to eliminate any counts due to photons. Secondly, the average dark current count per pixel for that length of exposure had to be obtained and subtracted. This second step prompted an investigation into the behaviour of dark current with varying exposure length and CCD temperature.

As dark current follows Poisson statistics, one can assume that its accumulation in the CCD (with no other restrictions presented to it such as pixel saturation) would be linear with time. For each pixel, every second there is a fixed probability that a dark current count will be measured. Therefore, by taking multiple dark frames of varying length for each temperature, a linear graph of mean pixel value against exposure length may be constructed. The gradient of this is simply the average dark current count per pixel per unit time.

Ideally, this value will be so small that a 0.12s bias frame would contribute negligible dark current counts per pixel.

Dark Frames

A dark frame is an image that represents the expected dark current for the exposure length that you are analysing. This is then subtracted from the image to provide a statistically dark current free image. A raw frame taken from the CCD with the absence of light is not a true dark frame however. The bias is subtracted from every dark frame in order for it to represent just the dark current present.

If we are happy with the assumption that dark current is linear with time, we can exploit this characteristic by generating a dark frame that corresponds to a much longer exposure than we are likely to take when observing the sky, scale it down to the exposure length and then subtract it. This long dark frame is called a scalable dark.

Dark current is dependent on temperature and so studies of dark current accumulation rate with temperature were performed and an appropriate working CCD temperature was obtained before a master scalable dark was produced.

In order to minimise the random fluctuation in dark current, it is beneficial to combine multiple dark frames by median filtering to create a master dark frame. The median is used over the mean for the averaging method because it has the added benefit of eliminating cosmic ray hits. These appear as high pixel count streaks or dots on the image, usually more than one pixel in size. They are caused by the subatomic particles travelling at high speeds that bombard the Earth constantly. As they are travelling with high momentum, they carry a significant amount of energy that, when passing through the CCD transferring some of their kinetic energy to the semiconductor, saturate several pixels around the point at which they hit. The mean would be skewed by this anomalously high value; the median is immune to this.

Flat Frames

The variations from a flat illuminated field of view due to the optics can be countered by dividing a frame by a normalised flat field. By taking a high signal to noise ratio image of a source of uniform illumination, an image of the variation from a flat field is recorded. This is known as a flat frame.

Dust particles, diffraction, external illumination operate as a multiplicative effect and so by dividing an image by a flat frame, these effects can be reduced significantly. Again, to reduce noise, many flat frames are taken, each with the master bias and scaled master dark frame subtracted, and then averaged together. The resulting frame is then normalised by dividing every pixel by the mean value of all of them. This way, for an area on the frame that experiences underexposure, it is divided by a value less than 1 thereby increasing it by the correct proportion. Similarly, an area of consistent overexposure is divided by a value greater than 1 to reduce its intensity.

New flat frames were taken for each observing session as dust can shift and external illumination change between observing sessions.

Defective Pixels

The previous year's study on the CCD revealed the existence of substantial pixel defects on the ST-7E in the form of hot pixels (pixels that over-count). These are immediately obvious as bright pixels on any dark frame longer than a couple of seconds. Approximately 10% were described to exhibit non-linear behaviour [11]. In order to fully understand the characteristics of these hot pixels and to verify the previous findings a variety of dark frames were taken. The main areas of investigation were how best to define when a pixel was hot or not, whether or not the hot pixels accumulated their charge in a linear fashion and whether their additional charge accumulation occurs during the exposure or if they exhibit an initial high value and then count normally.

In order to complete this analysis masks were made to represent each method of defining a bad pixel. Each mask consisted of a value 1 for a good pixel and a 0 value for pixel defined as bad. The name bad as opposed to hot was used so as not to rule out the possibility of pixels exhibiting a *cold* behaviour (a pixel that under-counts).

Three methods of masking were studied:

HOT MASKING

We assigned the title of a hot pixel to one whose mean value fell a certain number of standard deviations above the mean value of all pixels. This was attempted with 3 and 5 standard deviations. Most of these hot pixels were expected to be the bright pixels apparent in dark frames.

An iterative method was used, for example for the 5s.d. method, any pixel value above 5s.d. above the mean was masked out and so the data set decreased in size. It was then repeated until the value at which the cut-off occurred varied by less than 1 with successive iterations. Any pixel whose value fell above this final cut-off was assigned a mask value of 0 and anything below, a value 1.

WARM MASKING

A more rigorous approach that was devised was to make use of the Gaussian-like nature of Poisson statistics with high N. As dark current obeys Poisson statistics and the number of counts is high for long exposures, the distribution of pixel value with number of pixels per value tends to a Gaussian. It can then be assumed that, for a truly Poisson pixel, the probability of its value being above the mean for all the pixels is 0.5. The chance of this occurring twice in two observations, for that pixel, is $0.5^2 = 0.25$.

And so if we are to allow each pixel a 1 in the number of pixels on the array's chance of having a value above the mean every time for x observations, x would have to satisfy;

$$2^x = (765 \times 510)$$

$$x = \frac{\log 390150}{\log 2} = 18.52$$

Twenty half hour dark frames were taken and the pixels that fell above the mean in every frame were masked as bad. This way we can be statistically sure that these pixels exhibit non-Poisson behaviour.

Cool Masking

Using the same technique as the warm masking and the same 20 half hour exposures, pixels that record values below the mean every time were classed as 'cool pixels'.

CCD Temperature Stability

The CCD cooling was tested by monitoring the CCD's percentage of cooling capacity (displayed in CCDOps as a percentage) with decreasing temperature below the ambient temperature. A stable cooling temperature is required to ensure that the dark current values we subtract relate to the same temperature as the data it is subtracted from.

A cooling temperature was set and compared to the ambient room temperature taken with a lab thermometer. The percentage of cooling capacity and its variation was monitored and recorded.

Light Leakage

The process of taking dark frames to study dark current and defective pixels was performed in the observatory at day. The rubber lens cap on the CCD was kept on and the camera's mechanical shutter set to stay closed during exposure to retrieve a dark frame.

About halfway through the process of taking darks it was noticed that the average counts appeared to be decreasing throughout each experimental session. The ambient light was failing at the same time and so it was suggested that perhaps the CCD housing wasn't entirely light tight. Tests were done with the camera in varying orientations and in varying light conditions and it was decided that the darks be repeated in a light-tight dark room.

Photometry & Maskfix

Photometry is the process of obtaining a value for the flux output of a star. An evaluation of the counts from the source is determined by taking into careful consideration a number of factors such as the amount of background illumination in that patch of sky, the diameter of the Gaussian and any other atmospheric effects that alter the flux we receive at the telescope.

Aper

To perform photometry on a given star an IDL routine called Aper is used. The routine requires the user to input the x-y coordinates of the centre of the star's Gaussian and a set of radii within which photometry is to be calculated. An annulus at a larger radius is also set which is used to calculate the average background sky value. Aper then subtracts the sky value from the image and counts the remaining flux within each radius. A value is output for each radius.

With increasing radius the flux will increase at a reducing rate until the radius stretches outside the majority of the star's Gaussian and all that remains is the random variation due to the Poisson noise in the sky counts which should average to zero (since the mean was subtracted). This plateau value was recorded as the total flux for that star that the CCD is receiving.

Maskfix

Aper's routine counts the values for all the pixels within a set radius. With the presence of the hot pixels the ST-7E provides, the Aper value of flux that is output is too high. The hot pixels raise the apparent magnitude of the star. A solution to replace the hot pixels with scientifically estimated values was required.

Maskfix is an IDL routine that was written for this specific issue in this project. It is a flexible routine that takes any image array and mask, of ones and zeros only and matching dimensions, and replaces the defined bad pixels (zeros in the mask) with the average of the good pixels around it.

It runs in a loop as many times as required fixing only pixels that are surrounded by at least 7 or 8 good pixels first and fixing the less 'available' pixels as they are freed up. It is also capable of handling the edge and corner pixels correctly. The result is an intelligently corrected image on which Aper can be run without overestimating the flux. See *Appendix 1. The MaskFix .pro File*.

Because of the extensive calculation performed by Maskfix along with the prioritising and repeat runs, a heavy mask can result in a long computation time (up to half an hour for some masks applied to an ST-7E image.

Observing Plans

In order to maximise the useful data taken during a night's observing it is important to make a plan of the evening's activities. A large number of objects for viewing are selected prior to the evening and their information organised. The right ascension and declination for each object is tabulated along with its name, a description of defining features (double stars of given separation, nebulous cloud, r' star for example) and the peak times at which it can be observed. An example info sheet for a list of double stars chosen to observe in a night is shown in **Table 1**.

OBJECT	SAO	RA	DEC	M1	M2
Gamma	92680	01 53 30	+19 18 00	4.8	4.8
40/41	8994	18 00 12	+80 00 00	5.7	6.1
Mu	30239	17 05 18	+54 28 00	5.7	5.7
39	45231	14 49 42	+48 43 00	6.2	6.9
S 3050	73656	23 59 30	+33 43 00	6.6	6.6
65	74295	00 49 54	+27 43 00	6.3	6.3
S 1633	82254	12 20 42	+27 03 00	7	7.1
E-Gem 38	96265	06 54 36	+13 11 00	7.4	7.7
OBJECT	**Separation**	**Comment**	**Peak Observing Times**		
Gamma	7.8	Equal	7-9 setting fast		
40/41	19.3	Equal	All Night		
Mu	2	Equal	All Night, Higher later		
39	2.9	Neat pair	All Night, Higher later		
S 3050	1.6	Equal	7-9 setting fast		
65	4.4	Equal	7-9 setting fast		
S 1633	9	Very pretty, solitary	9-2 Rising		
E-Gem 38	7.1	Equal	9		

Table 1 – An info sheet on selected double stars for the observing session of 7th March 2011.

An object is at its best observing location for a night when it's at its highest altitude with low ambient light. A web based tool called Staralt [12] was used to calculate which objects had their best visibility at good times for observing throughout the evening.

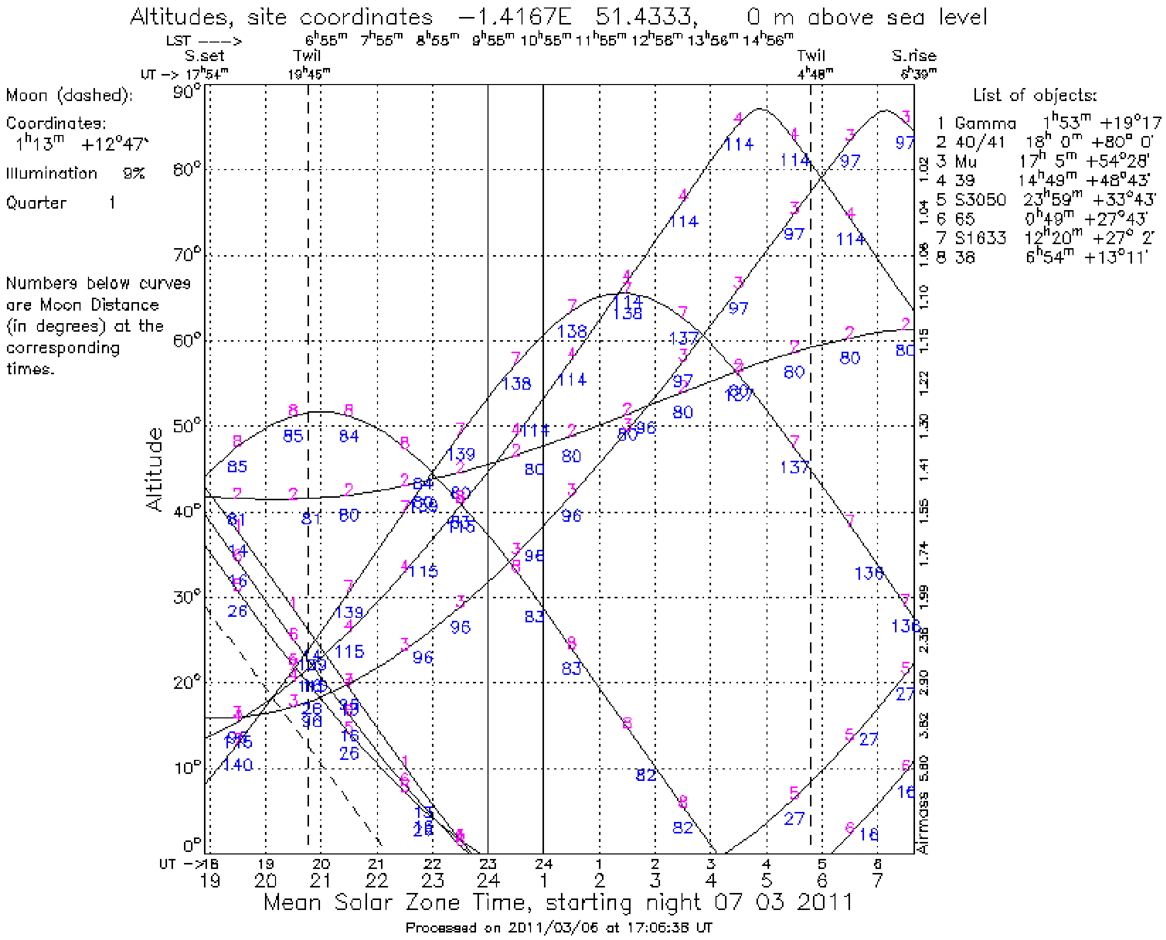

Figure 5 – A Staralt plot of the double stars listed in **Table 1**. The peak observing times for most objects are ascertained with a Staralt plot such as this.

A generalised plan of an evening's observations would consist of setting up the equipment prior to astronomical twilight (the time at which the centre refracted image of the Sun is 18° below the horizon and all ambient light is dark enough to perform any astronomical observation [13]).

4. Results, Analysis & Developments

CCD Testing

The first set of results collected was to test the temperature stability of the CCD with increasing percentage of cooling capacity used. The ambient temperature was 16.2°C and the cooling temperature was set to a range of values down to -12°C. The results are displayed in **Figure 6**.

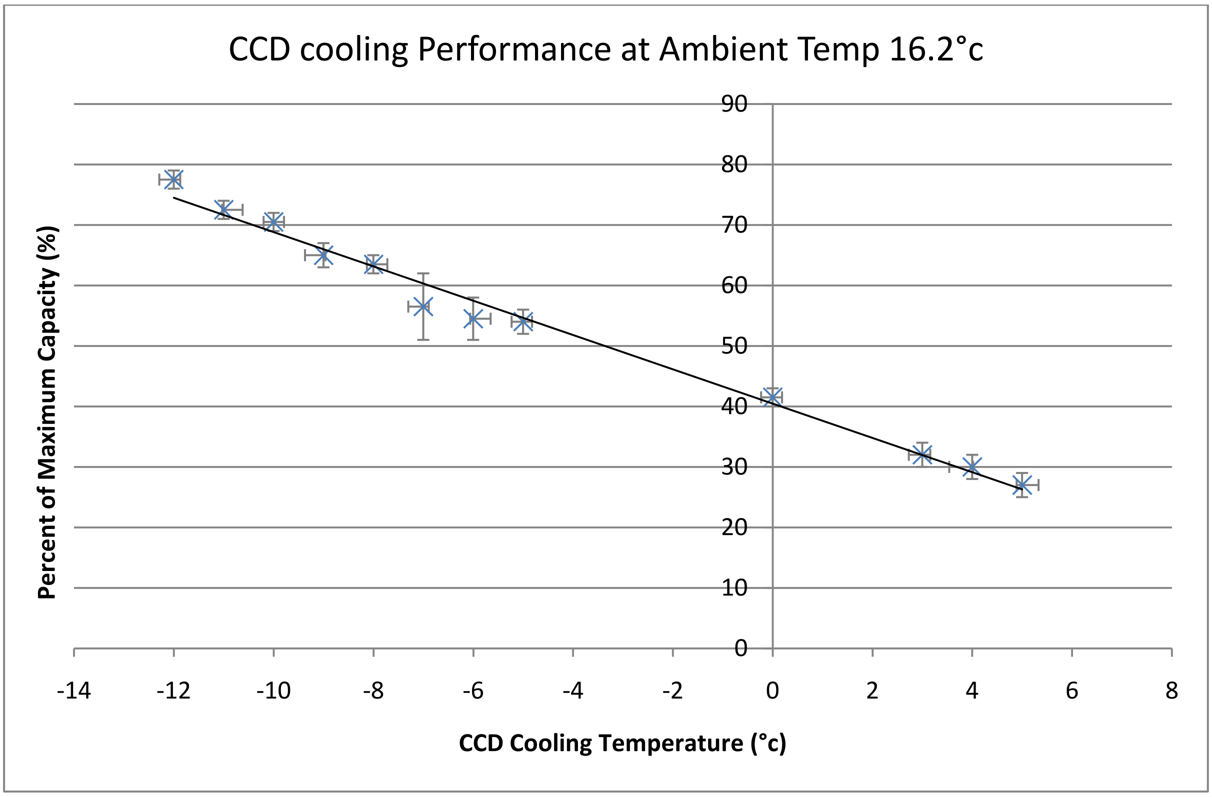

Figure 6 – CCD cooling performance to 28.2°C below ambient temperature.

The experimentation to ascertain a suitable CCD cooling temperature for observations consisted of dark frames of 4 exposure lengths (5,10,20 and 30 seconds) at temperatures from -15°C in 5 degree intervals up to ambient (+14°C). The gradients of the graphs provide a value for dark current counts per second. However this data was taken in light conditions and leakage rendered the data unreliable. None the less, it was noted that the gradients for the -15,-10 and -5 degree data were very similar. The data was repeated in darkroom conditions but, with a higher ambient temperature, the lowest cooling temperature obtained was -5°C. The data is shown in **Figure 7** below.

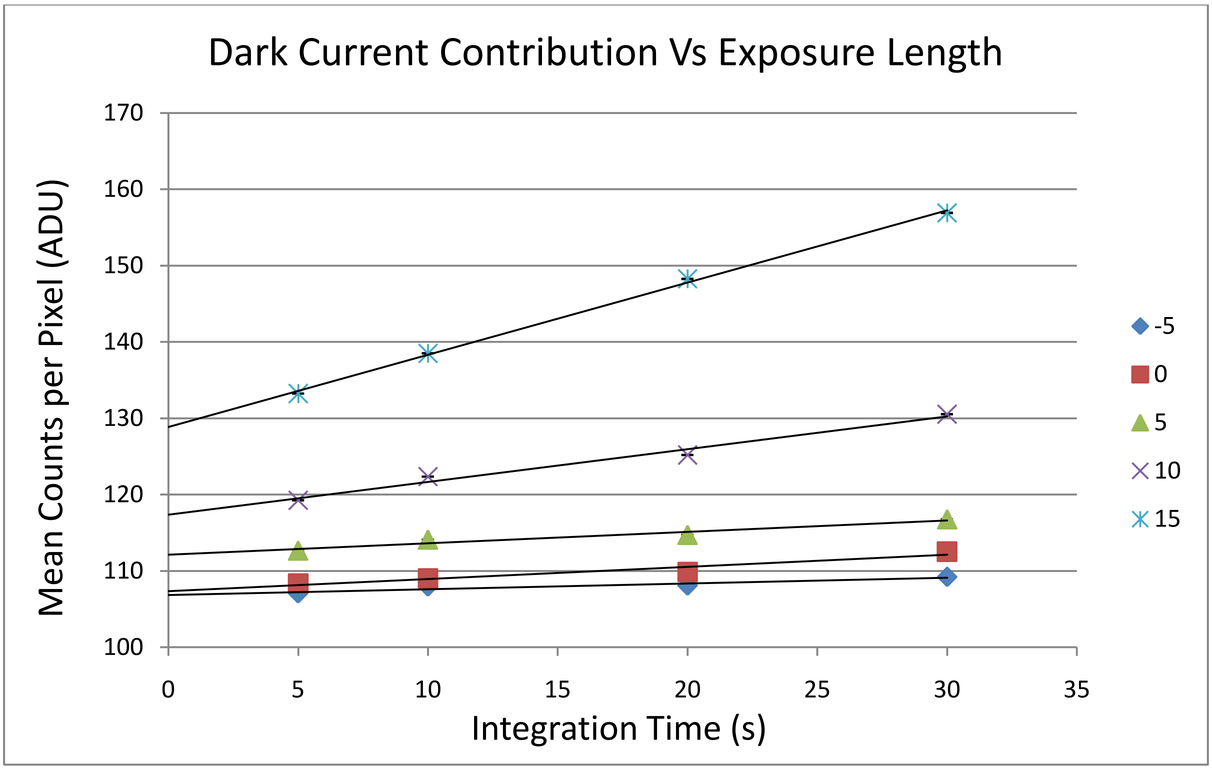

Figure 7 – Rate of dark current accumulation with varying CCD cooling temperature.

The justifiability of implementing scalable master darks hangs on the linear accumulation of dark current. Although the results in **Figure 7** contain the data to argue this linearity, a more rigorous investigation was desired. A larger range of exposure lengths were taken under darkroom conditions at 0°C and -5°C. See **Figure 8**.

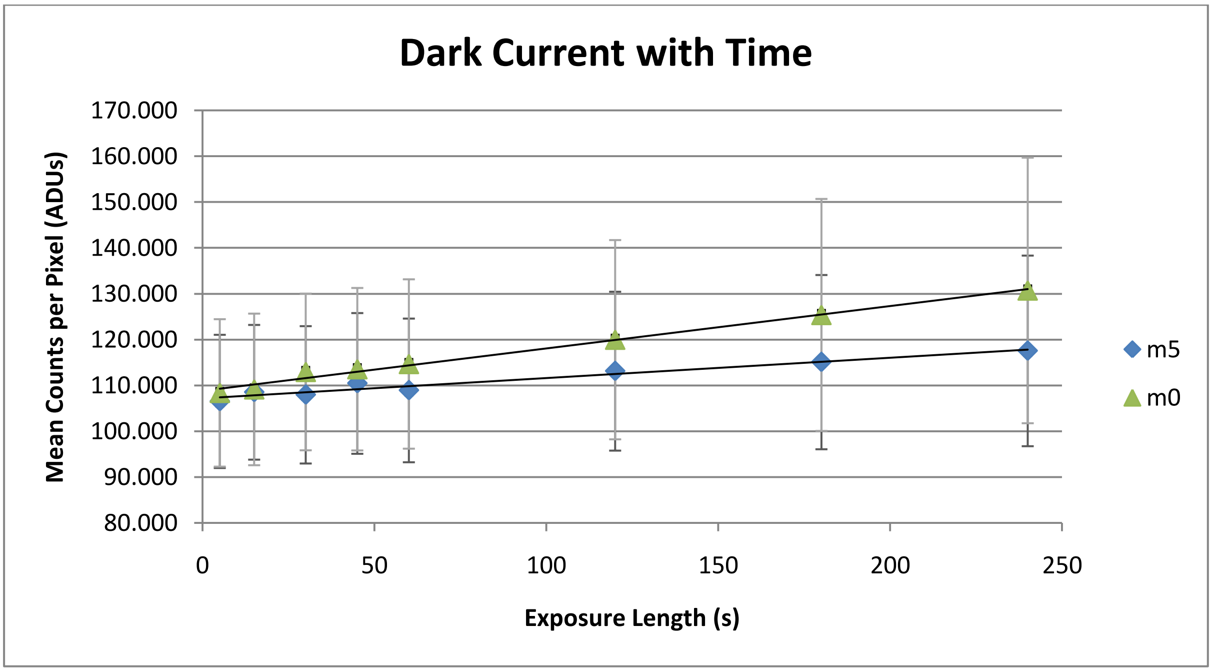

Figure 8 – The average pixel value for dark exposures of varying length at two temperatures. The error bars are 2 standard deviations of the data. Poisson errors could not be used as the data includes the CCD bias and hot pixels which are not Poisson in nature.

The linearity of photon detection with time was also tested through varying length exposures of the star SAO96265. It was found that pixels accumulated photon counts linearly up to the saturation point.

The master bias frame can be analysed for structure that may not be visually apparent. If found it could lead to an explanation for the origin of some of the noise the bias frame exhibits. This is done by performing a 2D fast-Fourier-transform (FFT) on the frame. This represents the image in terms of discrete frequencies which itself takes the form of an image (the central pixel is the longest wavelength while the outside pixels represent the shortest). Any periodic pattern will show up as prominent features in the FFT. The master bias frame produced exhibited no pattern in the FFT and as such we can conclude that it consists of pure random noise.

A histogram of pixel values for a long dark exhibited a non-Gaussian shape. The hot pixels that appear as bright spots on any frame present themselves as a secondary bump at higher pixel values. The Gaussian also appears to extend further into higher pixel values than lower values. It was this that flagged the possibility of warm pixels with values lower than the obvious hot pixels. Before attempting to generate the masks required to deal with these, a method of ascertaining whether their location on the CCD was constant was required.

A dark frame was chosen at random (call it dark A) and the histogram studied. A 'limiter' value was chosen by eye as the point at which the distribution began to depart from a Gaussian. Another dark was chosen (dark B) and a histogram of the pixels in dark B where dark A's values fell below the limiting value was plotted. If the hot and warm pixels' locations are constant, one would expect the histogram to appear distinctly more like a Gaussian. A composite of dark B's histogram with and without the limiting is shown in **Figure 9**.

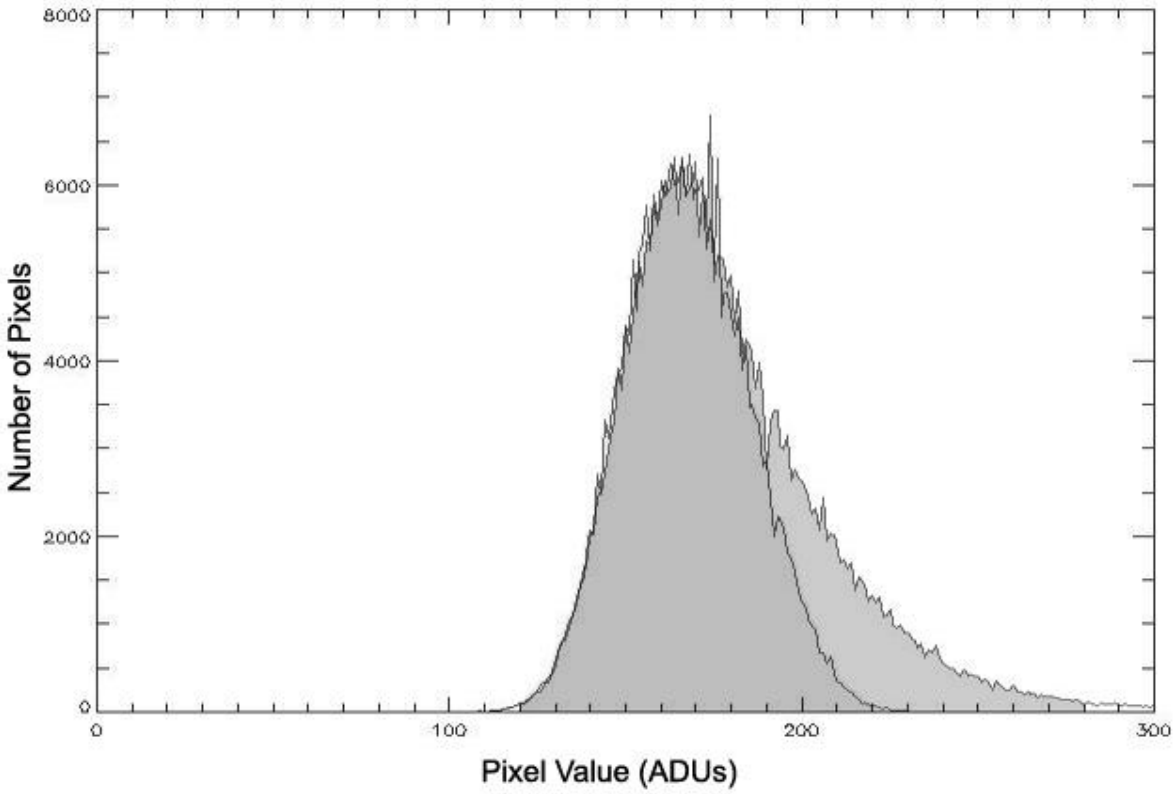

Figure 9 – The overlaid histograms of the same dark frame with and without a limiting mask made from another dark applied. The distribution with a more Gaussian shape is the data with the limiter mask applied, the other with the positive tail is the raw data's histogram.

In order to make the three levels of masking the twenty half-hour dark frames were taken in the darkroom. The CCD operating temperature decided on was -5°C. The hot, warm and cool pixel masking operations were performed on the resulting median filtered array of all 20 darks.

Since the masks consist of ones for good pixels and zeros for masked pixels, the total of the mask is the number of good pixels. Following this, the proportion of the CCD that is masked is calculated; **Table 2**.

Pixels Masked	Percentage of CCD masked
Hot	9.31
Hot & Warm	45.12
Hot, Warm & Cool	53.40

Table 2 – The level of masking as a result of each technique.

With the aid of the masks produced, the characteristics of the bad pixels can analysed separately from the good pixels.

It was decided that the hot pixels would have values that that would saturate at useful length exposures of the sky. These pixels would always have to be corrected with the Maskfix routine or ignored entirely. The warm pixels, however, were only slightly higher in counts than expected. Experimentation was performed to decide whether their increased charge accumulation could be rectified when a scaled dark frame was subtracted from the image.

Twenty dark frames of one minute exposure were bias subtracted and median filtered. Four thirty minute dark frames were also bias subtracted, median filtered and then scaled down by a factor of thirty to simulate a one minute exposure. One was then subtracted from the other. The result is displayed in **Figure 10**.

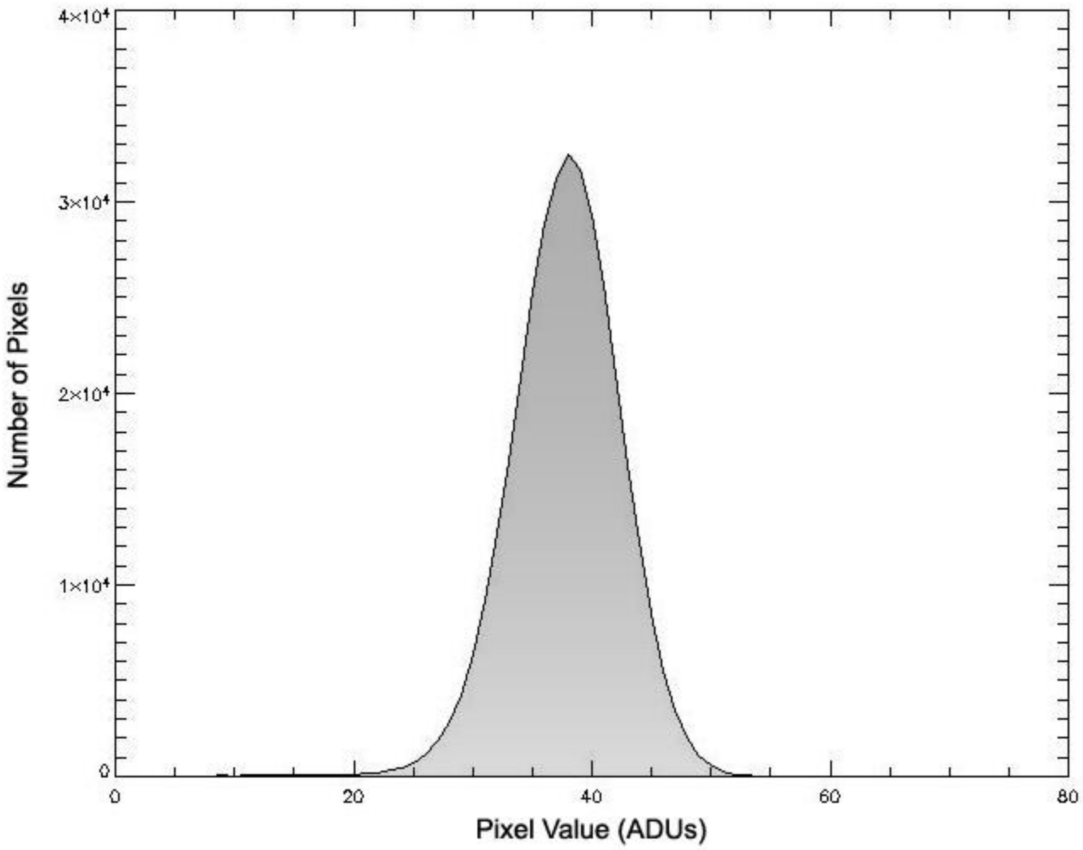

Figure 10 – The result of subtracting a 1min exposure from a scaled down 30min exposure (both bias subtracted). The deviation from a Gaussian is visible as a slight negative skew. The graph has been shifted along the x-axis by +40 such that 40 represents zero.

PHOTOMETRY

With evidence to suggest that dark subtraction would not correct for the warm pixels the next question was; for a star's image with a large number of counts, would the error due to the warm and cool pixels fall within the errors due to other factors such as seeing and count statistics?

In order to answer this question, photometry was performed on two stars for an unmasked image and the three levels of masking. The stars were HIP31635 (a faint star that was used by the SDSS team in the calibration process of the r' filter) **Figure 11** and Maia (a bright star in the Pleiades cluster) **Figure 12**.

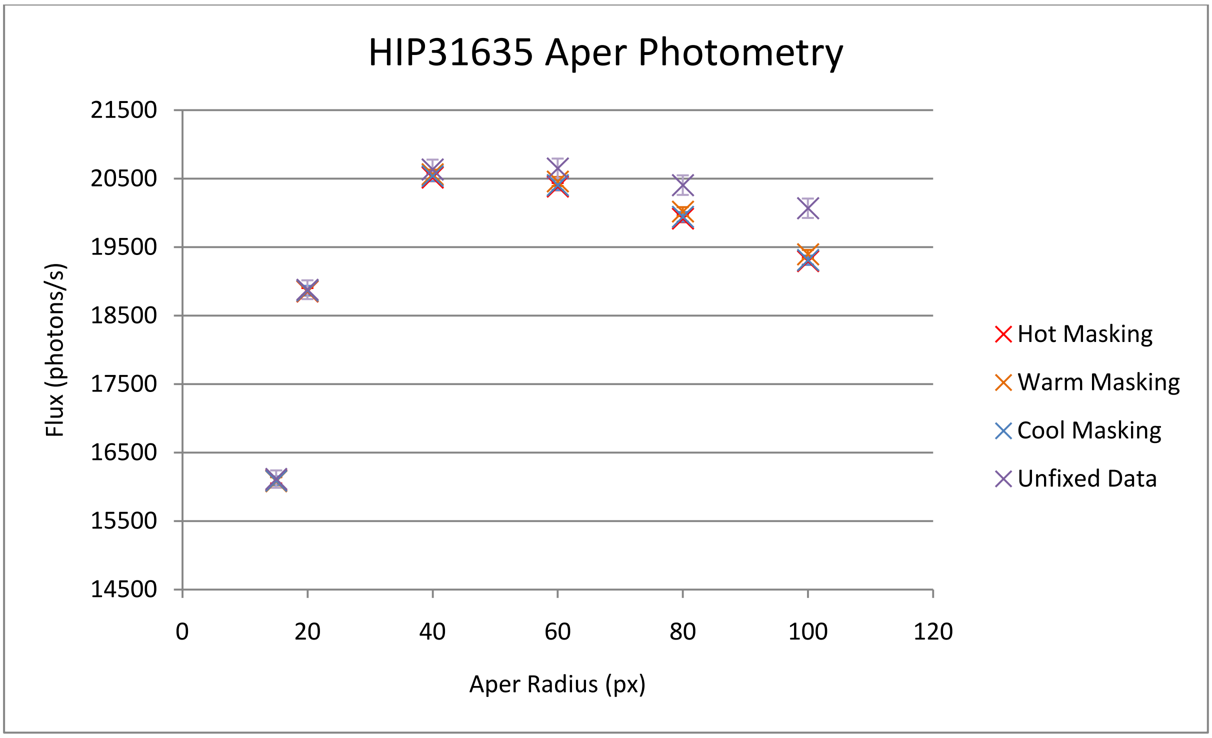

Figure 11 – Aper photometry on the r' standard star HIP 31635. Photometry for the three levels of masking along with the un-maskfixed image is displayed. Their errors are calculated by running the custom Aper-like IDL program on the remaining (unmasked) pixels and taking the result's Poisson error.

The r' magnitude value for each star was obtained with a particular form of **equation (3)** for the $AB_{r'}$ system;

$$m_{r'}(\lambda) = -2.5 \log F_{r'}(\lambda) - 48.6 \tag{5}$$

Which is justified since the AB magnitude with an r' filter is equal to the r' magnitude, $r' = r'(AB) + 0.0$ (SDSS base their filter system on the AB system) [14]. The subtracted constant in **equation (5)** is a zero point to align a particular chosen flux as a magnitude 0 object. $F_v(\lambda)$ is the flux corresponding to a band centred at λ measured in $erg\ s^{-1}\ cm^{-2}\ Hz^{-1}$.

The value, N, measured at the CCD is in counts and so a number of corrections and conversions are made to manipulate the value into the correct flux units. Combining the Planck relation and wave relation for a photon of wavelength of the centre of the filter we obtain;

$$F_{r'} = \frac{Nhc}{\lambda}\frac{1}{tA}\frac{\lambda}{c} = \frac{Nh}{At} \tag{6}$$

The Planck's constant is $h = 6.63 \times 10^{-27} erg\ s$, A is the effective collecting area of the telescope and t is the exposure length in seconds.

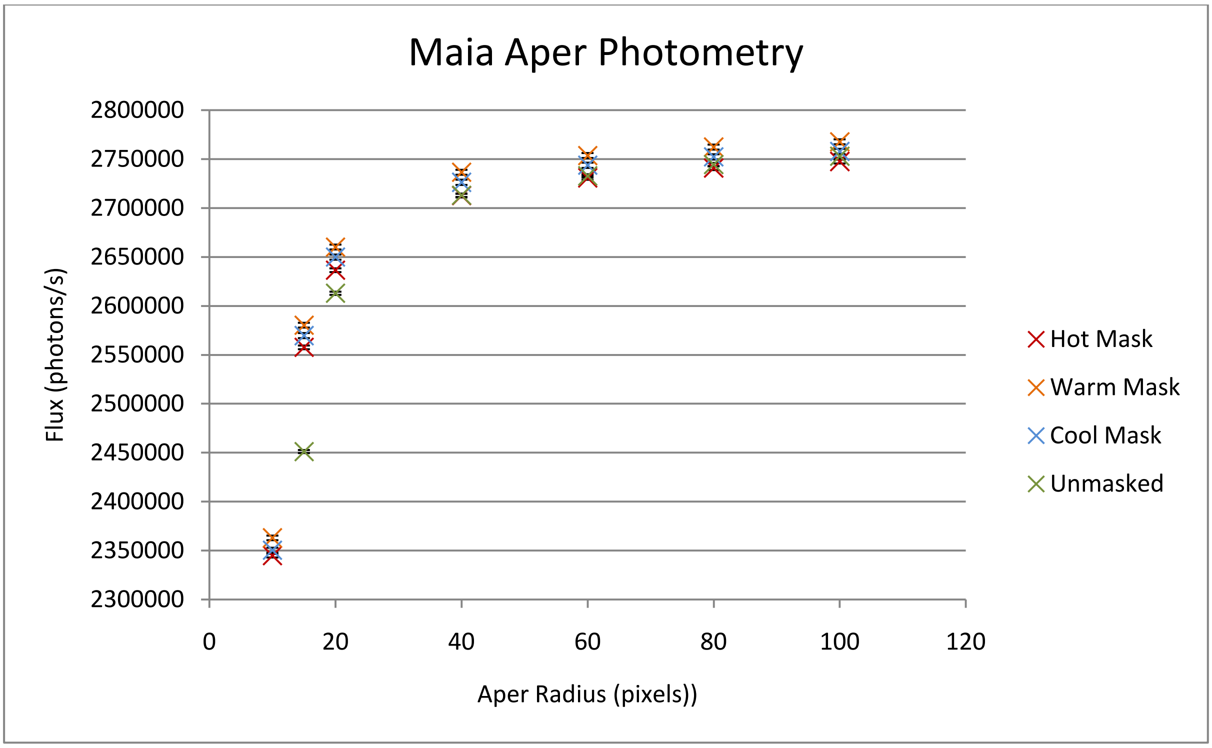

Figure 12 - Aper photometry on Maia in the Pleiades cluster. As with the r' in **Figure 11**, the photometry on all three mask fixed images, along with the raw image, are shown.

The same method was applied to other stars to obtain their fluxes using just the hot mask, their magnitudes were calculated and tabulated along with their altitude, theoretical r' magnitude and the difference between the theoretical and experimental values (see **Appendix 2**).

A plot of the air mass with the difference between theoretical and experimental magnitudes was constructed (**Figure 13**) and displayed the expected straight linear relationship.

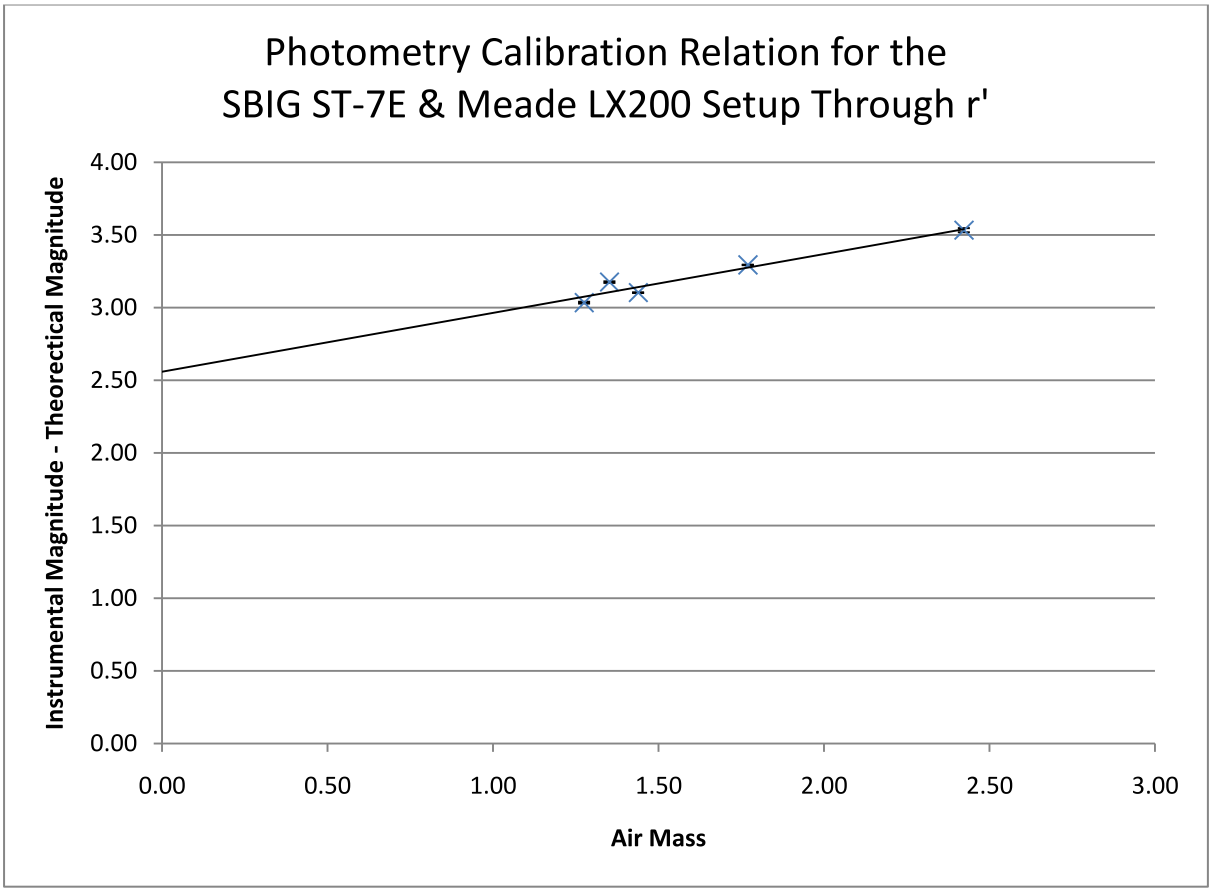

Figure 13 – A plot of the calibration values for each object with air mass.

A 'least-squares' fit to the data provides a zero air mass magnitude, m_0, and extinction coefficient, k, along with their errors:

$$m_0 = 2.560 \pm 0.005$$

$$k = 0.405 \pm 0.002$$

Resolving Power

The double star, E GEM, in **Table 1** was the smallest separation binary observed with an angular separation of 7.1 arcseconds. The images taken were analysed in the astronomy software 'SAOImage DS9'. A projection was performed through the line connecting the two stars. The projection was given a width of 3.0 pixels in an attempt to average out the slight fluctuations from a Gaussian across each star's profile. The projection area is shown in **Figure 14** below on the left along with its plot on the right.

As discussed on page 8 the FWHM of the seeing disk is a measurement of seeing, another limiting factor on the resolving power. The 'gauss2Dfit' routine in IDL fits a 2-dimensional Gaussian to a 2D array. This was used for several stars and the parameters of the Gaussian fit recorded. The table of results is shown in **Appendix 3**.

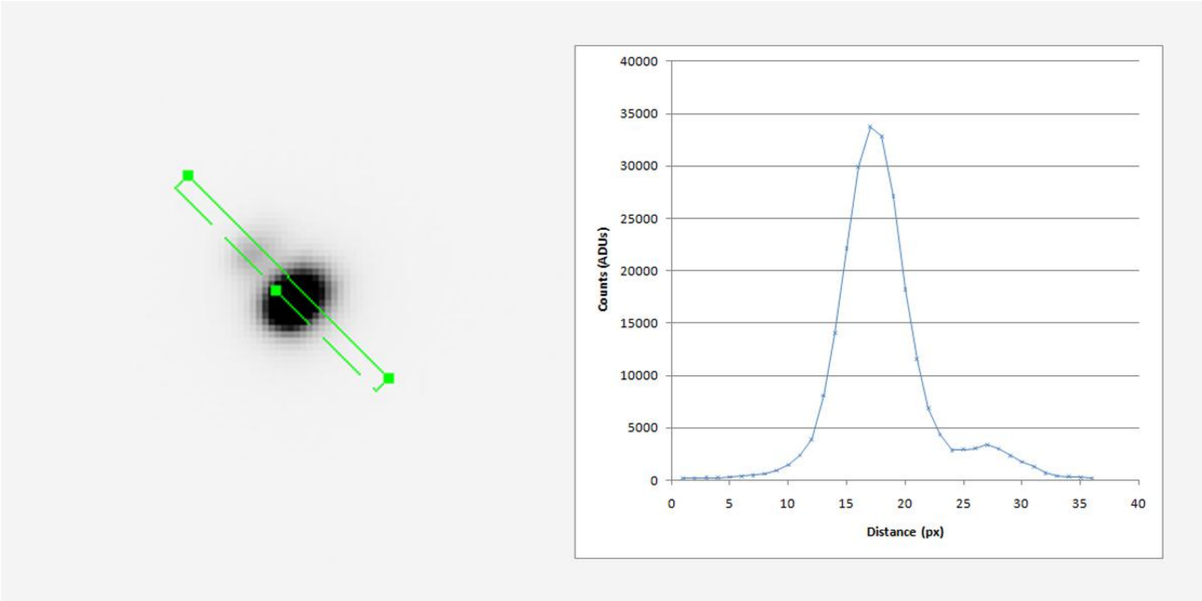

Figure 14 – The projection across the E Gem double star with angular separation of 7.1". The image and the area of projection is shown on the left while the projection itself is shown on the right.

STACKING

Extended objects were also imaged during the observations. The Orion nebula (M42) features a cluster of bright stars interspersed by nebulous gas that has a luminosity substantially dimmer than that of the stars. In order for the CCD not to saturate, a short exposure of 5 seconds was used. This resulted in a low signal-to-noise ratio for the gas. The improvement in the SNR is the square root of the number of stacked images [15]. In order to bring out the details of the gas structure stacking of 7 images was attempted, producing an effective exposure of 35 seconds. The effect of stacking is shown in **Figure 15**.

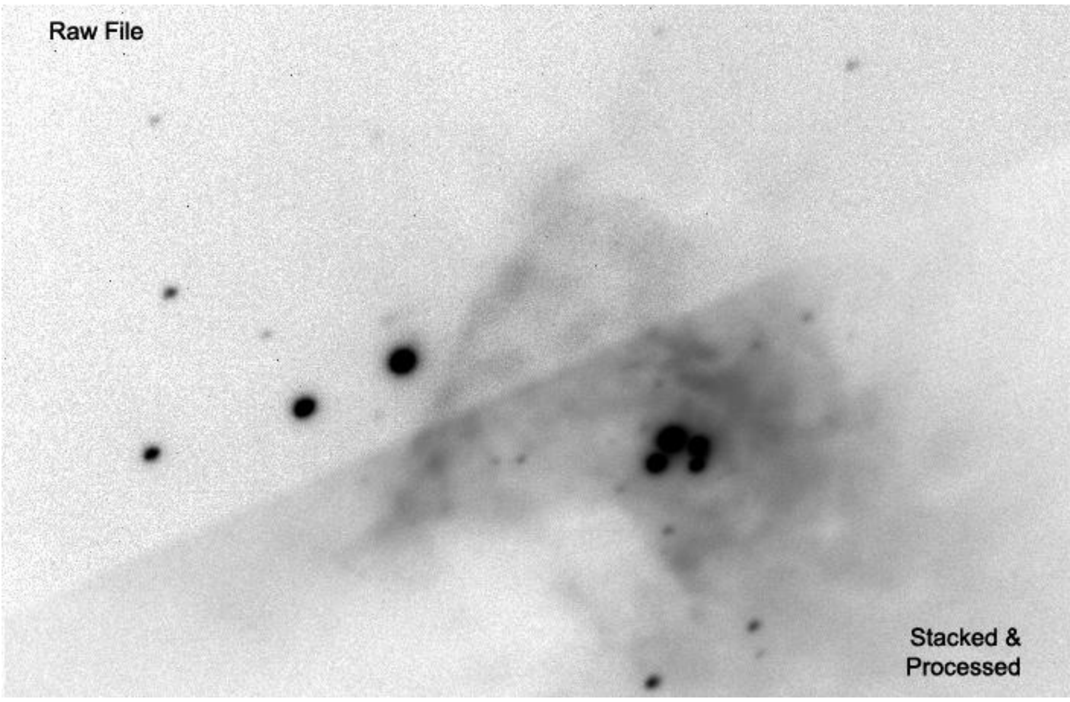

Figure 15 – A comparison negative image of the effects of stacking. Top left is the raw file while the bottom right is the result of stacking 7 images. The final image has also been Maskfixed and dark and bias subtracted.

5. DISCUSSION

CCD ANALYSIS

The ST-7E's characteristics were tested extensively under varying temperatures, exposure lengths and varying intensities of illumination.

Basic characteristics such as the linear accumulation of dark current with time along with the stability of the cooling at varying cooling temperatures were investigated. **Figure 7** & **Figure 8** display the linear dark current time relation and also lead to the conclusion that -5°C was a suitable operating temperature both in terms of dark current rate and CCD stability at most ambient temperatures. Later observations confirmed this.

Further developments have been made on understanding the extent of pixel behaviour distributions. The hot pixels acknowledged in last year's project have been identified as making up 9.31% of the CCD. This number was obtained in a more rigorous manor (iterative 5 standard deviation method) than in the previous attempt. The results show a consequential improvement on the approximate figure of ~10% obtained using a single 3 standard deviation cut-off last year [11] [16].

The behaviour of a further 44.09% of the pixels have been identified as non-linear in behaviour and methods of dealing with this departure from the expected Poisson statistics have been explored. The idea of subtracting a scaled dark frame from the data in order to correct the warm or cool behaviour of these pixels proved not to work as the resulting distribution of the dark current was not a symmetrical Gaussian about zero as shown in **Figure 10**. The Maskfix program was then written as an alternative solution. This program is flexible, easy to use and can be made available for use in future projects.

PHOTOMETRY

It was shown that consistent photometry could be performed on images of stars, particularly making use of the new r' Sloan filter. An instrumental magnitude was obtained for a number of sources. Their offset from a theoretical value and atmospheric extinction was fully quantified.

Theoretical values of r' magnitudes for all photometry objects were obtained from a SIMBAD (online star database) search of their B and V magnitudes. Instrumental magnitudes of the stars were calculated taking into consideration ADU to photon conversion, CCD quantum efficiency and background signal. The remaining variation from the theoretical value was studied and a strong relationship between air mass at the time of observation and deviation from theory was found. A least-squares fit of this relationship has provided two parameters of complete calibration of the telescope. The y-intercept, a, is the remaining instrumental offset at zero air mass due to undetermined factors. The gradient, b, is the extinction coefficient for this filter and observatory.

The undetermined factors of the y-intercept are likely a composition of characteristics of the telescope setup such as correcting lens and filter transmission percentage, absorption by the mirrors or errors in factored values. This is not a problem as they are contained in the single calibration value.

In order to perform the photometry measurements, Maskfix was used on each image. It was shown that, after correcting the 9.31% hot pixels, further mask based pixel fixing didn't change the flux value significantly and as such is superfluous for magnitude calculations.

As the Maskfix routine introduces simulated flux counts to pixels, they must be discounted in error calculations. It was understood that Aper is unable to cope with this requirement and thus an alternative form of aperture photometry was written and implemented **Appendix 4**.

NYQUIST/DIFFRACTION/SEEING LIMITS

As expected, it was found that the most limiting factor to the resolving power of the telescope on the nights of observation was the seeing which, at its best, was 3.46 arcseconds. It is anticipated that seeing at the observatory would never approach the limits imposed by either diffraction or CCD resolution.

With a Nyquist limit associated with 2 pixels and an image scale as defined by **equation (3)**, the resolving limit imposed by the CCD resolution is 2.32 arcseconds. This makes the Nyquist limit the next limitation of resolving power with the problem of seeing removed.

STACKING

The stacking of the images of M42 worked successfully, decreasing the SNR of the image thereby bringing out the detail in the dimmer features. Several dimmer stars were noticed after the stacking process, these could later be identified by a comparison of the field of view with virtual observatory software such as 'Microsoft Worldwide Telescope'; as shown in **Figure 16**. In future work this could enable the photometry of much fainter sources.

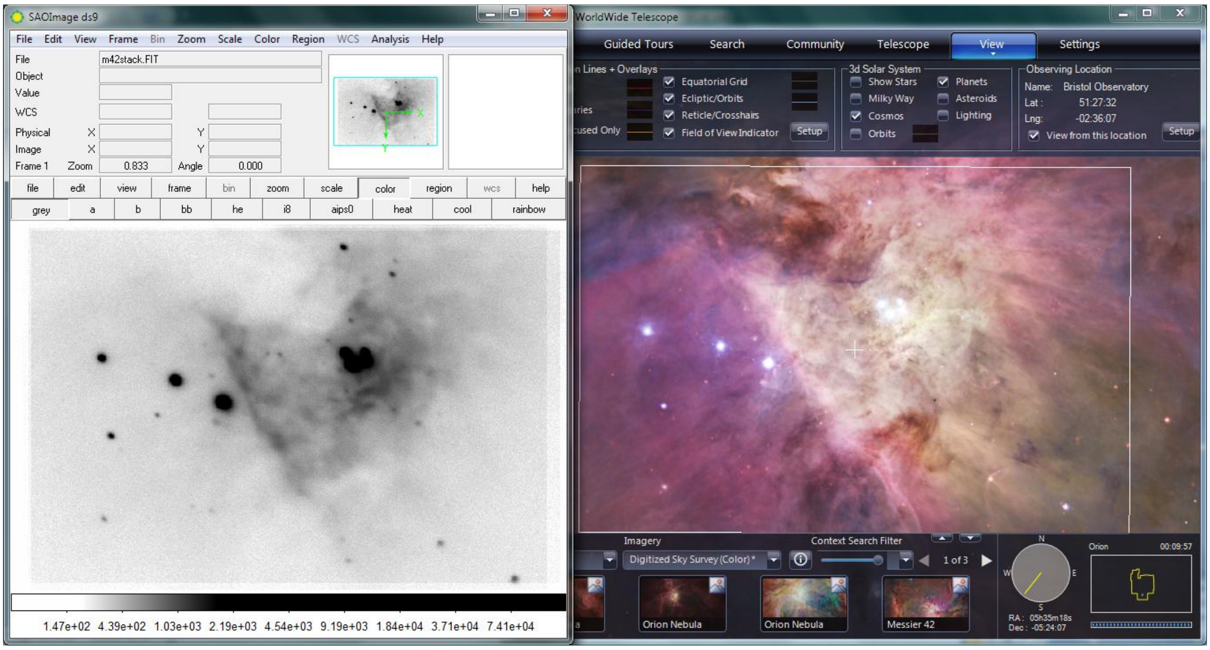

Figure 16 – A comparison of the stacked M42 image (left) and a Hubble Space Telescope picture overlay in Microsoft Worldwide Telescope (right). Notice the dim stars visible in the bright gas cloud on the stacked image which were not visible in a single frame and are also indistinguishable in the Hubble image due to the scaling of the gas luminosity.

Variable Stars

It was planned to take observations on variable stars to determine to what extent the setup was sensitive to fluctuations in star luminosities. One variable was attempted but due to tracking issues it was later ascertained that the wrong star was imaged. Ideally, observations over a longer timescale would need to be taken to build up an intensity variation profile of a star.

Potential for Further Work

Although an extinction coefficient and calibration value was calculated, it would be interesting and beneficial to take further photometry readings on other stars to test the values and pin down an expected error on r' values calculated using them.

An alternative method of obtaining the extinction coefficient is to take exposures of the same star throughout the night as it changes in altitude. This method could be performed to determine whether it agrees with the coefficient calculated here.

The analysis on seeing was brief in this project, mainly solely to confirm that it is the most limited factor on the resolving power of the telescope. It may be beneficial in the planning of future observation nights to take multiple measurements of seeing at different cardinal directions around the observatory. It is expected that the seeing to the North-West and at low altitudes will be particularly bad as a column of warm air rises from the Physics Department Nanoscience and Quantum Information supercomputer cooling system. If this effect could be quantified it could help plan resolving power dependent observation planning.

6. Conclusion

The work performed and explained in this report was intended to present a deeper understanding of the Coldrick optical observatory. It hasn't been a pursuit of a particular numerical value or physical model, rather an assessment, through careful analysis, of the potential of the observatory for future observing work.

The limiting factors of the location, CCD and telescope have been explored to reasonable depth and the previous year's work has been both confirmed and expanded upon. Most notably the hot pixels noticed previously have been precisely located and two more levels of pixel characteristics have been identified as warm and cool, explored and dealt with accordingly.

Full photometric calibration was performed through the Sloan r' filter and stacking trials have shown a potential for expansion in this area along. The promising results of photometry have opened doors to a significant study in variability of stars while a 360° map of the seeing around the observatory remains a profitable sideline.

APPENDICES

1. THE MASKFIX .PRO FILE

```
; NAME:
;   maskfix
;
; Author:
;   Will Foxall (Bristol University, BSc Physics 2011)
;
; PURPOSE:
;       Where a mask array of values 1 & 0 is equal to 0, the function
replaces
;   the like-indexed value in a data array of the same dimensions with
;    the average of the surrounding array values, including only the
values
;   for which the corresponding index mask value is 1.
;     The function is iterative such that it prioritizes for array values for
;   which the surrounding values in the mask array have the most 1s.
;        Designed to average over bad pixels in an image based on a
generated
;   mask where a 1 is a good pixel and 0 is a bad pixel.
;
; INPUTS:
;   dataarray   - Data array to be corrected.
;   maskarray   - Mask array of 1s and 0s.
;
; OUTPUTS:
;   result - The corrected array

function maskfix,dataarray,maskarray
;
; duplicate data and mask so as to make function non-destructive
data=dataarray
mask=maskarray
;
; Obtains the required dimension of the inputs
   sda = size( data )
   sma = size( mask )
   Lx = sda[1]-1
   Ly = sda[2]-1
;
; Check arrays match in dimensions
   if (sda[0] NE 2) OR (sda[4] LE 9) $
   OR (sma[1] ne sda[1]) OR (sma[2] ne sda[2]) then begin $
     message,"inputs must be images (matrices) of matching
dimensions",/INFO & $
;      return,data & $
   endif
;
; Check mask is just 0s and 1s
   if (MEAN(mask(where(mask ne 0)) - 1) ne 0) then begin $
     message,"maskarray must be composed of 0 and 1 values
only",/INFO & $
;      return,data & $
   endif
;
; Obtain the number of pixels to fix
   nbad = sma[4] - TOTAL(mask)
   if (nbad eq 0) OR (nbad gt 0.75*sma[4]) then begin $
     message,"mask 0% OR >75% 0s (perfect mask OR highly
inaccurate result)" & $
```

```
;      return,data & $
   endif
;
; Create array for bad pixel information (x,y coords and availability)
   info=intarr(3,nbad)
;
; Store x y coords of bad pixels
   i=0 & j=0 & $
   n=double(0) & $
   for i=0,lx do begin $
   for j=0,ly do begin $
     if (mask(i,j) eq 0) then begin $
       info(0,n)=i & $
       info(1,n)=j & $
       n++ & $
     endif & $
   endfor & $
   endfor
;
; Make an oversized data/mask array to prevent operations off edge of
array
odata=fltarr(lx+3,ly+3)
for i=1,lx+1 do begin $
for j=1,ly+1 do begin $
odata(i,j)=data(i-1,j-1) & $
endfor & $
endfor
;
omask=fltarr(lx+3,ly+3)
for i=1,lx+1 do begin $
for j=1,ly+1 do begin $
omask(i,j)=mask(i-1,j-1) & $
endfor & $
endfor
;
corrected=fltarr(nbad)
c=0L
;
;
WHILE (sma[4]-total(mask) gt 0) do begin

; Write availability of pixel
   for n=0L,(nbad-1) do begin $
   region=fltarr(3,3) & $
     if (info(2,n) ne -1) then begin $
       x=info(0,n) & $
       y=info(1,n) & $
       region(0,0)=omask(x,y) & $
       region(1,0)=omask(x+1,y) & $
       region(2,0)=omask(x+2,y) & $
       region(0,1)=omask(x,y+1) & $
       region(2,1)=omask(x+2,y+1) & $
       region(0,2)=omask(x,y+2) & $
       region(1,2)=omask(x+1,y+2) & $
       region(2,2)=omask(x+2,y+2) & $
       info(2,n)=TOTAL(region) & $
     endif &
     n=n+1 & $
   endfor & $
;
; Index order of collumn three in decending order (highest avail. first)
   order = REVERSE(SORT(info(2,*))) & $
   info = info(*,order) & $
;
; Start with maximum availability
   s = 8 & $
   While (max(info(2,*)) lt s AND s gt 0) do begin $
      s = s - 1 & $
```

```
   Endwhile & $
;
; Correct pixels for highest and second highest availability
   n = 0L & $
   region=fltarr(3,3) & $
   While (info(2,n) eq s) OR (info(2,n) eq s-1) do begin $
     x=info(0,n) & $
     y=info(1,n) & $
     region(0,0)=odata(x,y)*omask(x,y) & $
     region(1,0)=odata(x+1,y)*omask(x+1,y) & $
     region(2,0)=odata(x+2,y)*omask(x+2,y) & $
     region(0,1)=odata(x,y+1)*omask(x,y+1) & $
     region(2,1)=odata(x+2,y+1)*omask(x+2,y+1) & $
     region(0,2)=odata(x,y+2)*omask(x,y+2) & $
     region(1,2)=odata(x+1,y+2)*omask(x+1,y+2) & $
     region(2,2)=odata(x+2,y+2)*omask(x+2,y+2) & $
     odata(x+1,y+1)=TOTAL(region)/info(2,n) & $
     n=n+1 & $
     corrected(c)=odata(x+1,y+1) & $
     c++ & $
   endwhile & $
;
; Correct mask
   n = 0L & $
   While (info(2,n) eq s) OR (info(2,n) eq s-1) do begin $
     x=info(0,n) & $
     y=info(1,n) & $
     mask(x,y)=1 & $
     omask(x+1,y+1)=1 & $
     info(2,n)=-1 & $
     n++ & $
   endwhile & $
;
; Resort info array
   order = REVERSE(sort(info(2,*))) & $
   info = info(*,order) & $
endwhile

for i=0,lx do begin & $
for j=0,ly do begin & $
data(i,j) = odata(i+1,j+1) & $
endfor & $
endfor

return,data
end
```

2. PHOTOMETRY RESULTS

Date	Time of Central Obs	Object Name	Air Mass	HIP	Number of Exposures	r' (instr)	r' (instr) error	r' (theory)	Instr. & Theor. Difference	r' (calibrated)[1]
24/03/2011	23:31	r' Standard	2.42	31635	5	12.64	0.014272381	9.107	3.53	**9.10**
24/03/2011	20:08	Maia	1.77	17573	6	7.32	0.001792713	4.028	3.29	**4.05**
07/03/2011	20:20	E-Gem	1.28	33202	5	7.75	0.006096227	4.711	3.03	**4.67**
07/03/2011	22:21	Alkaid	1.35	67301	3	5.20	0.00528016	2.022	3.18	**2.09**
07/03/2011	20:34	Alioth	1.44	62956	3	4.97	0.002313378	1.869	3.10	**1.83**

3. SEEING READINGS

Date	Time	Object	Seeing	Standard Error
24.03.11	20:08	Maia	3.79	0.81
07.03.11	20:20	E Gem	3.46	0.75
24.03.11	23:31	HIP31635	8.78	3.68
07.03.11	21:00	Mintaka	5.15	3.21

[1] The calibrated r' value is obtained by applying the instrumental zero-point and extinction coefficient acquired with the least-squares fit to the r'(instr) value. i.e. $r'(calibrated) = r'(instr) - m_0 - kX$. *(See 16Results, Analysis & Developments: Photometry)*

4. Aper Photometry and Error Flux Calculation

```
a1=readfits('~/telescope_data/Observing/07.03.11/Plough/0_25plou
gh3_1.FIT')

flat=readfits('~/telescope_data/Observing/07.03.11/Flats/flat.FIT')
dark=readfits('~/telescope_data/masters/scaledmasterdark.FIT')
dark=dark/30
bias=readfits('~/telescope_data/masters/masterbias.FIT')

ab1=(a1-bias-dark)/flat

maskhot=readfits('~/telescope_data/masters/sig5mask.FIT')
maskwarm=readfits('~/telescope_data/masters/chmask.FIT')
maskcool=readfits('~/telescope_data/masters/chcmask.FIT')

.compile '~/telescope_data/maskfix/maskfixnospace.pro'

ma1=maskfix(ab1,maskhot)

mb1=maskfix(ab1,maskwarm)

mc1=maskfix(ab1,maskcool)


sharplim=[0.2,1.0]
roundlim=[-1.0,1.0]

find,ma1,x1,y1,flux1,s,r,120,8,roundlim,sharplim

; The located stars are sorted by flux intensity. The bightest star is the
r'

x1=x1(REVERSE(sort(flux1)))
y1=y1(REVERSE(sort(flux1)))
flux1=flux1(REVERSE(sort(flux1)))


; The x,y coords and flux of brightest star from each 'find' routine is
stored.

info=fltarr(3,3)
info(0,0)=x1(0)
info(1,0)=y1(0)
info(2,0)=flux1(0)

; Magnitude fixed data HOT MASK

; Divide by exposure length

ma1=ma1/0.25

skyrad=[100,120]
apr=[2,5,8,10,15,20,40,60,80,100]

APER,ma1,info(0,0),info(1,0),maga1,erra1,skya1,skyerra1,phpadu,apr,
skyrad,/FLUX

; Magnitude fixed data WARM MASK

skyrad=[100,120]
apr=[2,5,8,10,15,20,40,60,80,100]

mb1=mb1/0.25
```

```
APER,mb1,info(0,0),info(1,0),magb1,errb1,skyb1,skyerrb1,phpadu,ap
r,skyrad,/FLUX

; Magnitude fixed data COLD MASK

skyrad=[100,120]
apr=[2,5,8,10,15,20,40,60,80,100]

mc1=mc1/0.25

APER,mc1,info(0,0),info(1,0),magc1,errc1,skyc1,skyerrc1,phpadu,apr,
skyrad,/FLUX

; Magnitudes for RAW data

skyrad=[100,120]
apr=[2,5,8,10,15,20,40,60,80,100]

reduced1=ab1/0.25

APER,reduced1,info(0,0),info(1,0),magr1,errr1,skyr1,skyerrr1,phpadu
,apr,skyrad,/FLUX

; Multiply the image by the mask and perform Aper on that

hotmasked1=ab1*maskhot

warmmasked1=ab1*maskwarm

coolmasked1=ab1*maskcool

;--- Dist_circle method ---

dist_circle,circle1,[765,510],info(0,0),info(1,0)

; Hot masking

skyhotmasked1=Total(hotmasked1(where(circle1 gt 100 AND circle1
lt 120)))/Total(maskhot(where(circle1 gt 100 AND circle1 lt 120)))

hotmasked1=hotmasked1-skyhotmasked1

;Just turn the bad pixels back to zero. Now a good sky pixel will
average about zero (hopefully)
hotmasked1=hotmasked1*maskhot

print,total(hotmasked1(where(circle1 le 2))),$
total(hotmasked1(where(circle1 le 5))),$
total(hotmasked1(where(circle1 le 8))),$
total(hotmasked1(where(circle1 le 10))),$
total(hotmasked1(where(circle1 le 15))),$
total(hotmasked1(where(circle1 le 20))),$
total(hotmasked1(where(circle1 le 40))),$
total(hotmasked1(where(circle1 le 60))),$
total(hotmasked1(where(circle1 le 80))),$
total(hotmasked1(where(circle1 le 100)))

; Warm masking

skywarmmasked1=Total(warmmasked1(where(circle1 gt 100 AND
circle1 lt 120)))/Total(maskwarm(where(circle1 gt 100 AND circle1 lt
120)))

warmmasked1=warmmasked1-skywarmmasked1

warmmasked1=warmmasked1*maskwarm

print,total(warmmasked1(where(circle1 le 2))),$
```

```
total(warmmasked1(where(circle1 le 5))),$
total(warmmasked1(where(circle1 le 8))),$
total(warmmasked1(where(circle1 le 10))),$
total(warmmasked1(where(circle1 le 15))),$
total(warmmasked1(where(circle1 le 20))),$
total(warmmasked1(where(circle1 le 40))),$
total(warmmasked1(where(circle1 le 60))),$
total(warmmasked1(where(circle1 le 80))),$
total(warmmasked1(where(circle1 le 100)))


; Cool masking

skycoolmasked1=Total(coolmasked1(where(circle1 gt 100 AND circle1 lt 120)))/Total(maskcool(where(circle1 gt 100 AND circle1 lt 120)))

coolmasked1=coolmasked1-skycoolmasked1

coolmasked1=coolmasked1*maskcool

print,total(coolmasked1(where(circle1 le 2))),$
total(coolmasked1(where(circle1 le 5))),$
total(coolmasked1(where(circle1 le 8))),$
total(coolmasked1(where(circle1 le 10))),$
total(coolmasked1(where(circle1 le 15))),$
total(coolmasked1(where(circle1 le 20))),$
total(coolmasked1(where(circle1 le 40))),$
total(coolmasked1(where(circle1 le 60))),$
total(coolmasked1(where(circle1 le 80))),$
total(coolmasked1(where(circle1 le 100)))
```

REFERENCES

1. **University of Bristol.** Coldrick Observatory. *Bristol Astrophysics.* [Online] Department of Physics, 25 April 2006. [Cited: 27 April 2011.] http://www.star.bris.ac.uk/coldrick.html.

2. **S, Birney, G, Gonzalez and D, Oesper.** *Observational Astronomy.* Second Edition. Cambridge : Cambridge University Press, 2006. ISBN 0-521-85370-2.

3. **Meade Instruments Corporation.** *LX200 series Instruction Manual.* [Instruction Manual] Irvine : Meade Instruments Corporation.

4. **Meade Instruments Corp.** The Coma Killer. *Meade Instruments.* [Online] Meade Instruments Corp., 2006. http://www.meade.com/lx200-acf/coma.html.

5. **Sloan Digital Sky Survey.** SDSS Filters. *SDSS.* [Online] SDSS. http://skyserver.sdss3.org/dr8/en/proj/advanced/color/sdssfilters.asp.

6. **H, Bradt.** *Astronomy Methods.* Cambridge : Cambridge University Press, 2004. ISBN 0 521 535514.

7. **SBIG.** *Operating Manual, CCD Camera Models ST-7E, ST-8E, ST-9E, ST-10E and ST-1001E.* [Operating Manual] Santa Barbara : Santa Barbara Instrument Group, May 2001.

8. **Jacobsen, Dean.** CCD Image Calibration. *astrophoto.net.* [Online] 2009. http://astrophoto.net/calibration.htm.

9. **Quantum Scientific Imaging.** Understanding CCD Read Noise. *QSI.* [Online] Quantum Scientific Imaging, 2008. http://www.qsimaging.com/ccd_noise.html.

10. **Kodak.** KAF-0401E. *Brandeis University High Energy Physics Electronics Shop.* [Online] 2002. http://alignment.hep.brandeis.edu/electronics/Data/KAF0401E.pdf.

11. **Golding, M.** *Commissioning the Optical Telescope.* Department of Physics, The University of Bristol. Bristol : s.n., 2010.

12. **Azzar, Peter Sorensen and Marco.** Object Visibility. *Isaac Newton Group of Telescopes.* [Online] Isaac Newton Group of Telescopes, 2002. http://catserver.ing.iac.es/staralt/index.php.

13. **Weisstein, Eric W.** Astronomical Twilight. *Scienceworld.* [Online] Wolfram Research, 2007. http://scienceworld.wolfram.com/astronomy/AstronomicalTwilight.html.

14. **Wirth, Gregory D.** Astronomical Magnitude Systems. *Department of Physics & Astronomy.* [Online] University of Victoria, 2000. http://www.astro.utoronto.ca/~patton/astro/mags.html#conversions.

15. **Privett, G.** *Creating and Enhancing Digital Astro Images.* London : Springer, 2007. ISBN 978-1-84628-580-6.

16. **Huyton, P M.** *Calibration of the Department's Optical Telescope with Photometry.* Department of Physics, University of Bristol. Bristol : s.n., 2010.